PCCP
Physical Chemistry Chemical Physics

Accepted Manuscript

This article can be cited before page numbers have been issued, to do this please use: M. J. Amundarain, M. G. Herrera, F. Zamarreño, J. F. Viso, M. D. Costabel and V. I. Dodero, *Phys. Chem. Chem. Phys.*, 2019, DOI: 10.1039/C9CP02338K.

Molecular Mechanisms of 33-mer Gliadin Peptide Oligomerisation

Received 00th January 20xx,
Accepted 00th January 20xx

DOI: 10.1039/x0xx00000x

María Julia Amundarain [a], María Georgina Herrera†[b], Fernando Zamarreño[a], Juan Francisco Viso[a], Marcelo D. Costabel [a#] and Verónica I. Dodero[b#]

The proteolytical resistant 33-mer gliadin peptide is the immunodominant fragment in gluten and responsible for celiac disease, and other gluten-related disorders. Meanwhile, the primary structure of 33-mer is associated with the adaptive immune response in celiac patients, the structural transformation of 33-mer into protofilaments activates a primordial innate immune response in human macrophages. That means that accumulation, oligomerisation and structural transformation of 33-mer could be the unknown first event that triggers the disease. Herein, we reveal the early stepwise mechanism of 33-mer oligomerisation by combining multiple computational simulations, tyrosine cross-linking, fluorescence spectroscopy and circular dichroism experiments. Our theoretical findings demonstrated that the partial charge distribution along the 33-mer molecule together with the presence of glutamine that favours H-bonds between oligomers are the driving forces that trigger oligomerisation. The high content of proline is critical to forming the flexible PPII secondary structure that let to a β structure transition on oligomerisation. Experimentally, we stabilised the 33-mer small oligomers by dityrosine cross-linking, detecting from dimers to higher molecular weight oligomers, which confirmed our simulations. The relevance of 33-mer oligomers as triggers of disease as well as its inhibition may pose a novel therapeutic strategy for the treatment of gluten-related disorders.

Introduction

The 33-mer gliadin peptide, LQLQPFPQPQLP^{69}YPQPQLP^{76}YPQPQLP^{83}YPQPQPF, is a proteolytical resistant fragment of gliadin, which is a dietary protein found in the gluten of wheat, rye, barley and some varieties of oats. [1, 2] The incomplete proteolysis of 33-mer in humans was demonstrated by an analysis of human stool and urine, of subjects under gluten-containing diet, by using different ELISA methods. [3] It has been found that the 33-mer is the immunodominant peptide that triggers the adaptive immune response in celiac disease[4], but the early events of the disease, as well as the role of 33-mer in other gluten-related disorders, remain elusive. [2, 5] Importantly, the 33-mer gliadin peptide self-assembles with a structural transition forming nanostructures and protofilaments under physiologically relevant conditions. [6, 7] Moreover, it was shown that a radiolabelled 33-mer metabolite was accumulated in different organs in murine models, detecting monomers and high order aggregates *in vivo*. [8] Recently, it was demonstrated that large 33-mer supramolecular structures activate the innate immune response via a Toll-like receptor (TLR) mechanism, evidencing the role of 33-mer oligomers as early triggers of the disease.[9] In general, peptide/protein aggregates in combination with conformational transitions are the hallmark of misfolding diseases, including multiple sclerosis, Parkinson's disease, HIV-associated dementia, Alzheimer's disease, and Huntington disease, among others. In such conditions, a whole spectrum of possible aggregate species display distinct sizes and shapes and exhibit various degrees of toxicity. [10-14] There is evidence that the early oligomers in the process of aggregation might be considered more toxic than mature species such as fibrils or plaques. [14, 15]

Our hypothesis, in the context of gluten-related disorders, is that the persistence, accumulation, and oligomerisation of 33-mer per se might be an early event in the development of these diseases. Thus, any phenomenon inhibiting its oligomerisation may be considered as a possible new therapeutic target.

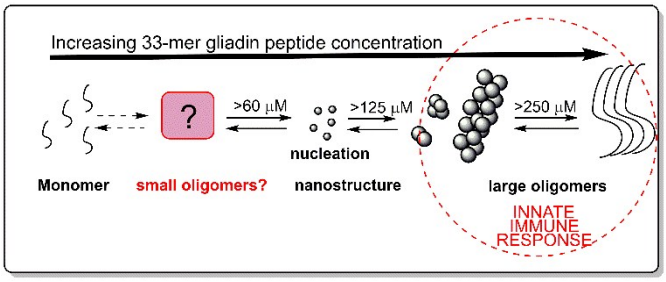

Scheme 1. Hypothetical 33-mer gliadin peptide oligomerisation pathway based on the state of the art.

Although the 33-mer high molecular weight (MW) oligomers are well characterised by electron microscopy, AFM, Helium microscopy and dynamic light scattering techniques, there is a lack of information about the initial stages of oligomerisation and its mechanism. [6, 7, 9,]

The main limitation is that 33-mer does not bind to any fluorescent dye, due to its high content of proline. Thus kinetic information of the early stages is not accessible by fluorescent detection methods.[16] Furthermore, 33-mer oligomerisation depends mainly on peptide concentration, and so far, at low peptide concentration, there is no experimental evidence of the existence of 33-mer small oligomers before the nucleation step (Scheme 1). Thus, the initial oligomerisation pathway of 33-mer remains elusive.

In the case of well-established amylogenic diseases, different modelling approaches were applied to their studies, such as

[a] Grupo de Biofísica, Instituto de Física del Sur, Universidad Nacional del Sur, Bahía Blanca, Buenos Aires, Argentina
[a.] Universität Bielefeld, Fakultät für Chemie, Organische Chemie, Universitätsstr. 25, 33615 Bielefeld, Germany
*Corresponding author: veronica.dodero@uni-bielefeld.de; costabel@criba.edu.ar
† Actual affiliation: Faculty of Pharmacy and Biochemistry, Institute of biological chemistry and Physicochemical, CONICET-University of Buenos Aires, Junín 956, C1113AAD, Buenos Aires (Argentina). Electronic Supplementary Information (ESI)

View Article Online
DOI: 10.1039/C9CP03738K

conventional molecular dynamic (MD) and replica-exchange, which have contributed to the understanding of the initial stages of oligomerisation for systems such as Aβ-42 peptide, [17] Amylin [18] and the prion protein PrP106–126. [19] By a preliminary MD model, it has been shown that 33-mer can form a dimer.[7] The present work aims to gain an understanding of the early steps of the 33-mer oligomerisation process combining *in silico* and *in vitro* experiments. First, we employed computational methods which include analysis of electrostatic properties together with atomistic and coarse-grained MD simulations showing the feasibility of a stepwise oligomerisation mechanism. During the simulations, we detected that Tyr 69 and Tyr 76 of two monomers are nearby less than 5Å. Thus a cross-linking reaction was experimentally performed under physiologically relevant conditions, obtaining for the first time stable covalent 33-mer oligomers from dimers to higher molecular weight oligomers at the lowest concentration of 50 μM, which is physiologically relevant.[1] Altogether, we obtained theoretical and experimental evidence of 33-mer oligomerisation that is driven by the peptide non-ionic polar character, flexible PPII secondary structure and its stabilisation by glutamine H-bonds.

Materials and Methods

Computational protocol

Model preparation and general protocol: The monomer model was prepared using the ABALONE software in a polyproline (PPII) structure, based on circular dichroism and nuclear magnetic resonance studies.[20]

Initially, to evaluate the aggregation propensity of 33-mer monomers into oligomers of larger size, we performed two atomistic simulations with ten monomers randomly distributed in an aqueous solution. All the starting structures were created by taking into account that the peptides should not overlap (Table S1 –SI). No clashes were found using the criteria for contacts in Chimera (a distance of two Van der Waals radii plus 0.4 Å). At the beginning of the production runs, it was corroborated that for every system, the interface between peptides/oligomers, was filled with water molecules. Also, a coarse-grained simulation with the same starting configuration was included to assess the stability of the aggregates by another computational tool (SI).

Finally, the stepwise aggregation of lower-order oligomers was assessed by atomistic MD simulations. Different starting configurations were assembled consisting of a monomer plus a lower order oligomer in different relative orientations. The distance between the peptides was initially at least as large as the sum of their Van der Waals radii and always consisted in elongated species (Table S2–SI). The electrostatic properties of the system were analysed, and from these results, hypothesis about the orientations that would favour aggregation was established and put into test through molecular dynamics simulations. We chose this approach to obtain oligomerisation, if possible, in accessible simulation times. In summary, MD simulations were performed assessing the behaviour of the peptides and oligomers in an aqueous solvent, by exploring their conformational space, and molecular patterns that favour oligomerisation. The detailed protocols are described below.

Electrostatic interactions: It has been well established that electrostatic interactions play a fundamental role in the determination of stability and function of bio-macromolecules. [21, 22] Therefore, an analysis of the electrostatic properties of the system was performed by solving the Poisson-Boltzmann (PB) equation, in all the structures to understand how these forces influence the self-organisation behaviour of the 33-mer peptide. The Adaptive Poisson-Boltzmann Solver (APBS) software package [23] was employed to solve the PB equation and model the electrostatic energy of interaction of the systems. This software solves the PB equation numerically by applying multigrid methods. In order to get the structures ready for the calculus and determine the protonation state of the peptides at physiological pH, PDB2PQR [24, 25] together with PROPKA [26, 27] were used applying the force field PARSE. [28, 29]

The simulation temperature was 310 K, and an implicit solvent was used (the presence of the solvent is modelled as a continuum with an empiric dielectric constant). A dielectric constant of 2 was assigned for the lattice points lying within the peptide and 78.5 for those within the aqueous phase region. The ionic strength was represented through ion species with opposite charges (1 C and -1 C respectively) and atomic radii of 2 modelled as 150mM of NaCl. Also, single Debye-Hückel boundary conditions were employed. The grid was determined for each system with the aid of APBS plug-in for Chimera, it was centred in the centre of mass of the system, and the length varied in such a way that the space between grid points was in average 0.49 ± 0.06 Å. The solutions of the PB equation obtained with APBS allowed us to construct maps of the equipotential surfaces and molecular surfaces coloured by potential. With the aid of the latter and careful visual inspection, hypotheses were made regarding the interacting regions. Additionally, the electrostatic profile of the monomer was analysed for pH 2, 7 and 9 (Table S3-SI). The different pH values are represented by changes in the protonation states of the residues, determined with PROPKA. [26, 27]

Molecular Dynamics: MD simulations have been used as a key tool to understand the mechanisms and the driven forces involved in the self-organisation process of many proteins and peptides. [30, 31] All the atomistic MD simulations were performed using GROMACS 4.6.5 package[32, 33] and the standard united-atom GROMOS53a6 force field. [34] The SPC/E model [35] was used for water molecules. Since the system is electrically-neutral, a concentration of 150 mM of NaCl ions was added. The protonation state of each amino acid is the one previously defined for pH 7 because it is the physiologically relevant pH. All the production simulations were carried out under the isobaric-isothermal (NPT) ensemble with imposed 3D periodic boundary conditions. A time step of 2 fs and the Leap Frog algorithm were used for integrating the equation of motion. The Nose-Hoover

algorithm [36, 37] was employed to keep the temperature at 310 K for the production runs, using coupling constant t_T=0.8 ps, and the Parrinello-Rahman barostat [38] to keep pressure isotropically constant at 1 bar, using a coupling constant t_T=2.0 ps and compressibility 4.5 10^5 bar^{-1}. Lennard-Jones interactions were cut off at a distance of 1.2 nm. For long-range electrostatics, the particle mesh Ewald (PME) method [39] was implemented with a real-space cut-off of 1.2 nm. LINCS algorithm [40] was applied to constrain all bonds to their correct lengths after an unconstrained update. The simulations were performed within a three-dimensional dodecahedral cell. The length of the box vectors was defined as the diameter of the system plus 2.8 nm; the detailed values for each system are presented in Table S2-SI.

To avoid the development of divergent forces, all the structures were minimised employing the steepest descent algorithm until the maximum force reached 200 kJ/mol.nm, with an initial step of 0.01 nm. Afterwards, a short simulation (200 ps) of the system in the NVT ensemble, at 310K, was performed while allowing the pressure to vary freely. The last equilibration step consisted of a 1 ns position restrained simulation in order to relax the solvent molecules around the peptides. For each system, 250 ns production runs were accomplished and then analysed with subprograms offered in the GROMACS package, namely *g_rama* (Ramachandran plots), *g_rms* (root mean square deviation), *g_sas* (solvent-accessible surface) and *g_gyrate* (radius of gyration).

To find the representative structure of each oligomer, clusterisation of the trajectories was performed with GROMACS *g_cluster*, using the Linkage method with a variable cut-off according to the simulation under study.

Possible hydrogen bonds were identified using geometric criteria, i.e., considering an acceptor-donor distance of 3Å and a cut-off for angles of 20 degrees, and selecting atoms that might act as donors and acceptors, as defined by Mills *et al.* [41] The secondary structure was estimated with STRIDE algorithm implemented in VMD. [42]

Experimental Procedures

Material:

The 33-mer gliadin peptide LQLQPFPQPQLP^{69}YPQPQLP^{76}Y PQPQLP^{83}YPQPQPF (3911 Da) with more than 95% purity was purchased to Biochem Shanghai Ltd lyophilised at different periods. Purity and mass were re-examined before experiments. Reverse-phase HPLC analysis was performed using a Venusil XBP C18 250 × 4.6. Binary gradients of solvents A (CH_3CN 0.1 %TFA) and B (H_2O 0.1%) were employed at a flow rate of 1.0 mL/min. The injection volume was 10 µL. HPLC peaks were detected by monitoring the UV absorbance at λ=220 nm, and the identity was confirmed by MS. The retention time of 12.023 min was obtained under the following experimental conditions: CH_3CN /H_2O with 0.1% TFA, 28-100%A 25 min. HPLC-MS (ESI): *m/z* 1958.61 $(M^+ + 2H)^{2+}$, 1305.16 $(M^+ + 3H)^{3+}$. Accurate Mass determination has been performed by ESI nano-MS: Measured Ion Mass $(M^+ + 4H)^{4+}$: 978.26472 (deviation 0.10) and Calculated Ion Mass: 978.26463 (deviation 0.11); Molecular Formula Obtained (C190H273N43O47) H4+4.

Tyrosine Crosslinking of 33-mer peptide oligomers

This experiment was performed to stabilise covalently the predicted *in silico* oligomers. The reaction was performed for a final peptide concentration of 50 µM in a total volume of 1 ml of 100 mM borate buffer pH 8.8 at 37°C. Briefly, the 33-mer gliadin peptide solution was prepared by taking an aliquot from a freshly prepared peptide stock solution in water and added in a borate buffer pH 8.8. Horseradish peroxidase Type VI (Sigma) was prepared in a stock solution in 10 mM phosphate buffer pH 7.4 and added to the 33-mer solution in borate buffer to obtain a final enzyme concentration of 0.3 µM. The volume was completed with MilliQ, and the reaction was started adding an aliquot of hydrogen peroxide to obtain its final concentration of 1 mM. Then, the reaction was maintained at 37°C for two hours and stopped adding a concentrated aliquot of Tris-Cl at pH 7.4 (50 mM).

Fluorescence Spectroscopy

Emission spectra of tyrosine and dityrosine before and after the crosslinking reaction were acquired at 25 °C. For this purpose, the 50 µM of 33-mer gliadin peptide solution was excited at 274 nm and 320 nm, tyrosine and dityrosine excitation maxima, respectively. For kinetic experiments, the sample was excited only at 320 nm, and the fluorescence emission spectra were recorded at 407 nm during 2 hours at 37°C. Experiments were performed in an FP-8300 fluorescence spectrometer from Jasco using bandwidth for the excitation and emission of 5 nm.

Separation and analysis of cross-linked 33-mer oligomers by denaturant acrylamide electrophoresis

The peptide solution was prepared at a final concentration of 50 µM as explained above, taking samples at 10, 20, 30 and 1 hour where the oxidative reaction was quenched with Tris.HCl pH 7.4 (100 mM). Then the samples were dissolved in urea at a final concentration of 8 M to disrupt other possible interactions and concentrated 50 times using an Amicon centricon with a cut off of 3kDa (Millipore). This protocol was perform to concentrate the sample and favour their detection. After this procedure, the sample was mixed with the sample buffer using 3.1 volume ratio, and subsequently, the resulting mixture was boiled for 5 min at 100 °C. The SDS electrophoresis analysis was performed using the Bio-Rad Mini-Protean chamber (Bio-Rad) under constant voltage (200 V). The separation gel consisted of 10–20% Mini-PROTEAN® Tris-Tricine Gel, from Bio-Rad. Electrophoresis buffer for the cathode was 100 mM Tris-HCl, 100 mM Tricine, 0.1% (w/v) SDS at pH 8.3 and the anode buffer was 200 mM Tris-HCl at pH 8.9. The sample buffer composition was 8 % SDS, 20% glycerol, 10% 2-mercaptoethanol, 0.002% Coomassie blue G250 and 100 mM Tris- HCl (pH 6.8). Two protein marker standards (BioRad) with a range of 1.400–26000 Da and 10000- 250000 Da were run alongside the samples. The gel was stained using a Zn staining protocol. [43] The gel analysis was performed using Image J, and the image montage was done with PhotoScape.

Circular Dichroism: CD spectra of 50 µM of 33-mer gliadin peptide in 100 mM borate buffer pH 8.8 in the absence or presence of horseradish peroxidase (0.3 µM final concentration) were acquired in a Jasco-810 CD spectrometer using a Peltier system

as a temperature controller. The CD spectra of the 33-mer oligomers after the cross-linking reaction were also acquired. CD temperature dependent experiments were performed from -5°C, 10°C, 25°C and 37°C. Five scans were acquired in the range of 190–250 nm at a selected temperature with an incubation time of 5 min. A scanning speed of 50 nm per minute was applied, and 1 mm and 0.1 mm quartz cuvettes were used, for native oligomers and cross-linked ones, respectively. For all the experiments, the corresponding buffer solutions were analysed under the same conditions and subtracted from the sample spectra. Smooth noise reduction was applied using a Savitzky-Golay method. Graphics were represented using the program Origin (Originlab Software).

Results

The in silico modelling of 33-mer oligomerisation propensity and structural transformation

To explore the 33-mer oligomerisation propensity and conformational space of 33-mer oligomers, two different atomistic MD simulations of 10 monomers randomly distributed in water were performed (SI, Table S1-S2). Both initial conformations were unbiased. The units employed were obtained from the previously reported 33-mer monomer model with a polyproline II (PPII) motif.[7]

In Figure 1, we present the 250 ns MD simulation, which converges after 50 ns to a stable decamer, as shown in the root-mean-square deviation (RSMD) plot. During the evolution of the simulation, it was observed a stepwise aggregation of the monomers into a decamer. During the first 50 ns of simulation, we detected an extended monomer, a dimer and heptamer (Figure 1B). Finally, these initial structures assembled into a stable decamer (representative snapshot Figure 1C). This process was evidenced in the solvent accessible surface (SAS) plot which displayed a marked decline in the exposed surface during the first 60 ns of the simulation and then a plateau which accounts for the stability of the newly formed aggregate (Figure 1D). The convergence of the simulation was corroborated with RSMD plot (Figure 1E). Taking a 0.30 nm cut-off, 202 clusters could be formed for the simulation, with the largest cluster containing 81% of the total structures and an RMSD of 0.45 nm between the most representative structure (Figure 1C) and the rest of the members of the group.

The Ramachandran histogram showed that in the explored conformations, there was an increase of β-like content and decrease of the initial PPII motif (Figure 1F and Fig S1). The secondary structure per residue of the representative frame of the first 100 ns of the trajectory indicates that internal sequence ^{71}QPQL has a conserved β secondary structure (between 60- 80%); meanwhile, ^{83}YP and the C-terminal F remain in PPII structure in the entire simulation (Fig. S2).

Both the intermediate states and the final oligomer displayed electrostatic potential and hydrophobic patterns compatible with further aggregation propensity. The final decamer is mainly hydrophilic, which justifies the formation of stable soluble oligomers in water (Figures 2 B-C). [6,7]

To evaluate whether a different initial configuration would also reproduce aggregation, another MD simulation of 10 randomly oriented monomers at longer inter-peptide distances (for details see SI, Fig S3) was performed. This resulted in the aggregation, in less than 100 ns, of an octamer and two isolated monomers.

To check the 33-mer oligomerisation propensity with a different computational molecular description, a coarse grained simulation was performed and described in the SI. In this simulation; a decamer was formed by the approach of the 33-mer monomers in the first nanoseconds of the entire 1 μs production run (for details see SI, Fig S4).

Altogether, these findings strongly suggest that the formation of stable high-order oligomers, such as decamers and hexamers are possible, and also that it is statistically feasible that monomers and dimers coexist with larger aggregates. Moreover, these results support our previous experimental observation that there is a conformational equilibrium between PPII and beta structure, favouring the formation of the later due to oligomerisation. [6, 7]The detection of monomeric and dimeric species in the ten-monomer simulation motivated the study of the plausible stepwise oligomerisation of 33-mer.

Evaluating the stepwise mechanism of 33-mer oligomerisation

By this approach, the sequential formation of higher-order oligomers was studied (see Table S1 and S2). The electrostatic profiles of the 33-mer monomer and the oligomers were analysed to identify the regions with higher propensity to establish interactions with other monomers. By this procedure, the starting configuration of each ensemble was selected, and atomistic MD simulations were performed. In each simulation, the ensemble was generated by the addition of a monomer to the previous obtained oligomeric structure.

The first analysis of the monomer showed that the electrostatic potential of the peptide was not affected by changes in the pH (2, 7 and 9 values were analysed) (see Table S3). This is consistent with the presence of non-ionic lateral chains in the peptide. For physiological pH and PARSE force-field, the potential distribution on the molecular surface of the monomer is shown in Figure 2A.

View Article Online
DOI: 10.1039/C9CP02338K

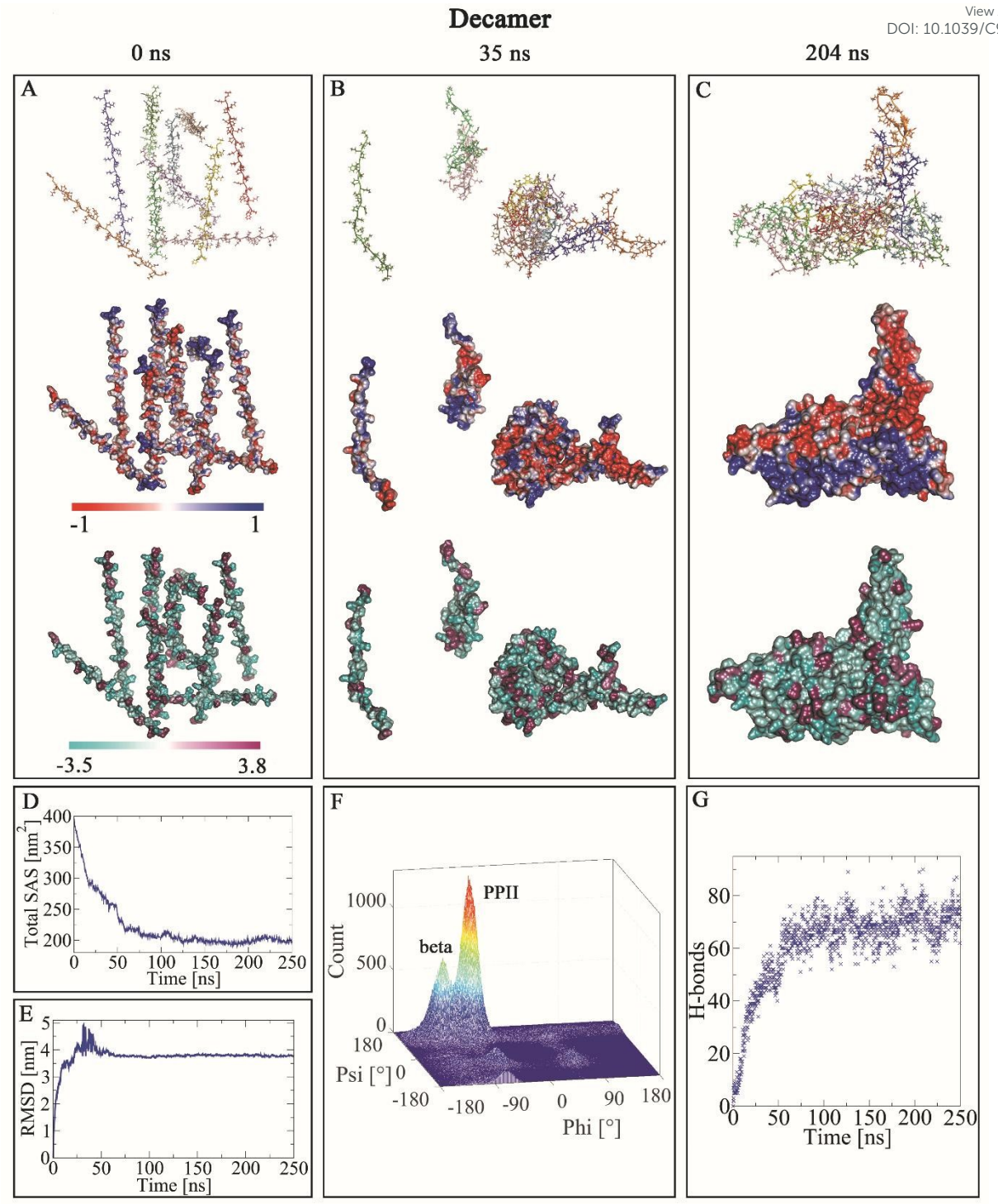

Figure 1. (A) Initial disposition of ten monomers in a solvated box depicted with licorice and the molecular surface coloured according to the electrostatic potential (measured in kBT/e) and the hydrophobicity (according to Kyte and Doolittle in cyan the more hydrophilic and in maroon the most hydrophobic residues). (B) The intermediate state of aggregation in which a monomer, a dimer and a heptamer evolve independently. (C) A representative structure of the principal cluster obtained from the atomistic MD simulation of the decamer. (D) The Solvent Accessible Surface area for the all-atom simulation of ten monomers displays four distinct regions, the first one represents the first assemblies of a heptamer and a dimer, the second one describes the evolution of these systems, the third stage shows how these three oligomers blend into one decamer which continues to increase its compactness in the latter region. (E) The RMSD evidences the stability of the oligomer after ~60 ns. (F) The Ramachandran histogram clearly shows two peaks in the PPII and beta regions. (G) The number of H-bonds during the trajectory is representative of the aggregation process.

This model evidenced 33-mer amphipathic nature, suggesting that the particular distribution of partial charges along the molecule in the PPII secondary structure is the intrinsic characteristic of 33-mer peptide that promotes its oligomerisation. The subsequent 250 ns MD simulation showed three stages of folding in which the peptide monomer remained mainly elongated for the first 20 ns (Fig. 2B-C) and then folded into increasing compact structures (Fig. 2D-E), as represented in the SAS plot (Fig. 2F). This behaviour suggested that it is possible that different monomeric species co-exist in equilibrium.

The simulation converged after 100 ns (Fig. 2G). The dihedral angles adopted by the residues in the trajectory belong mainly to PPII and β-like structures (Fig. 2H).

Based on the probability of finding elongated monomers in the decamer simulation, two elongated peptides were selected to model the dimerisation. The electrostatic analysis of the interaction between two monomers showed that all the tested configurations had negative electrostatic energies of interaction.

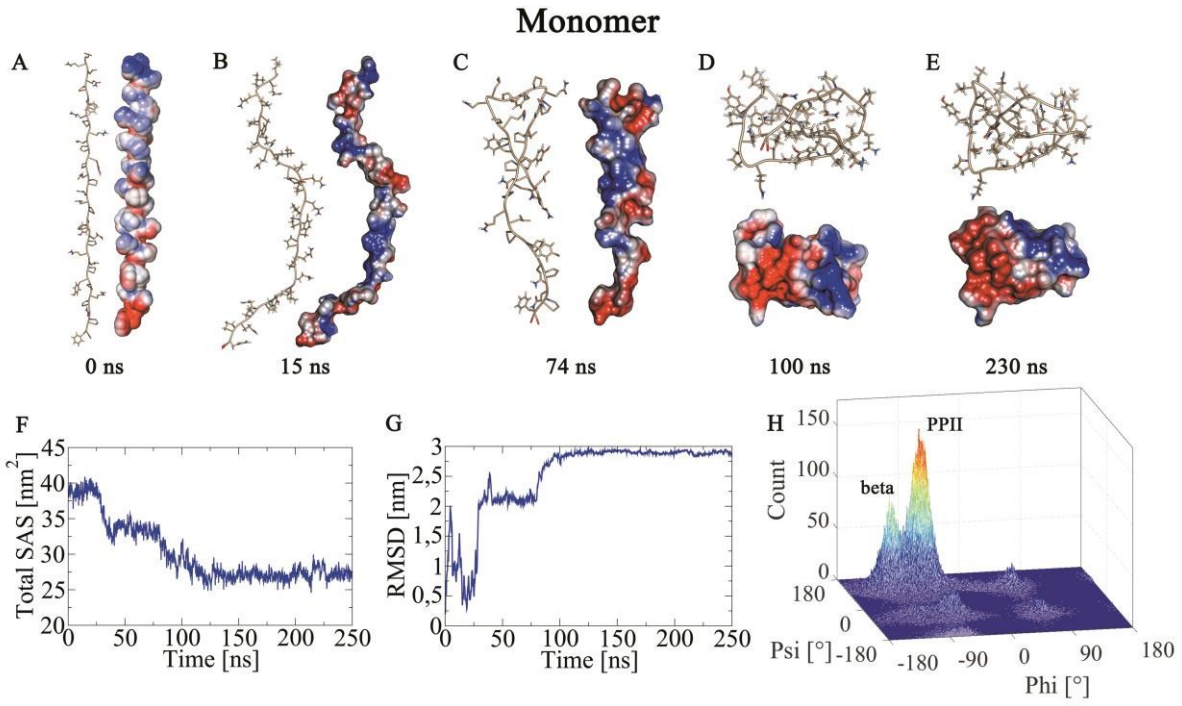

Figure 2. (A-E) Structural evolution of the monomer depicted with liquorice and through the molecular surfaces coloured by the electrostatic potential. Blue surfaces correspond to values 1kBT/e, white surfaces to 0 kBT/e and red surfaces to -1kBT/e Additional orientations are in Fig S6. (F) The Solvent Accessible Surface Area for the MD simulation is a measure of the packing of the structure; three distinct stages can be identified with different degrees of folding of the peptide (for the radius of gyration refer to Fig. S5). (G) The Root means square deviation shows the convergence of the simulation after 100ns. (H) Ramachandran histogram shows an increase in β-like content in the final structure (see Fig. S16A).

Thus, all of them could potentially form dimers. In order to promote aggregation, the configuration with the lowest electrostatic interaction energy was chosen. This was formed by two monomers oriented in an antiparallel fashion. This orientation had been observed in the second simulation of ten monomers (Fig S3). The MD simulations revealed that the dimer was formed after a few nanoseconds of the production run (Fig. 3A). The dimer remained elongated in the first part of the simulation, but then adopted a semi-folded conformation (Fig. 3A and S7). This evolution is evidenced in the SAS graphic and radius of gyration shown in Figures 3A and S8, respectively. The production trajectory, which reached convergence after 200 ns, was clustered into 153 groups, of which only two contained 52% of the total structures. The biggest cluster contained 31% of all the structures with an RMSD of 0.28 nm among the mean structure and the other members. This cluster represents elongated configurations. The second cluster, however, represents semi-folded conformations and contains 21% of the total structures, with an inter-cluster RMSD of 0.28 nm. These configurations are stabilized by several intra and inter-molecular H-bonds (see Tables S4-S5 and Fig S9).

Following the same trend and motivated by the formation of a dimer, the aggregation into a trimer of an elongated monomer and the dimer in a stable conformation was assessed (Fig 3B). The initial configuration was based on electrostatic compatibility from visual inspection of the electrostatic potentials. During the MD simulation, the dimer and monomer rapidly approached each other to form an initial structure of a trimer. The SAS in Figure 3B is consistent with the visualisation of the trajectories, the RMSD and the gyration radius charts (Fig. S10

View Article Online
DOI: 10.1039/C9CP02338K

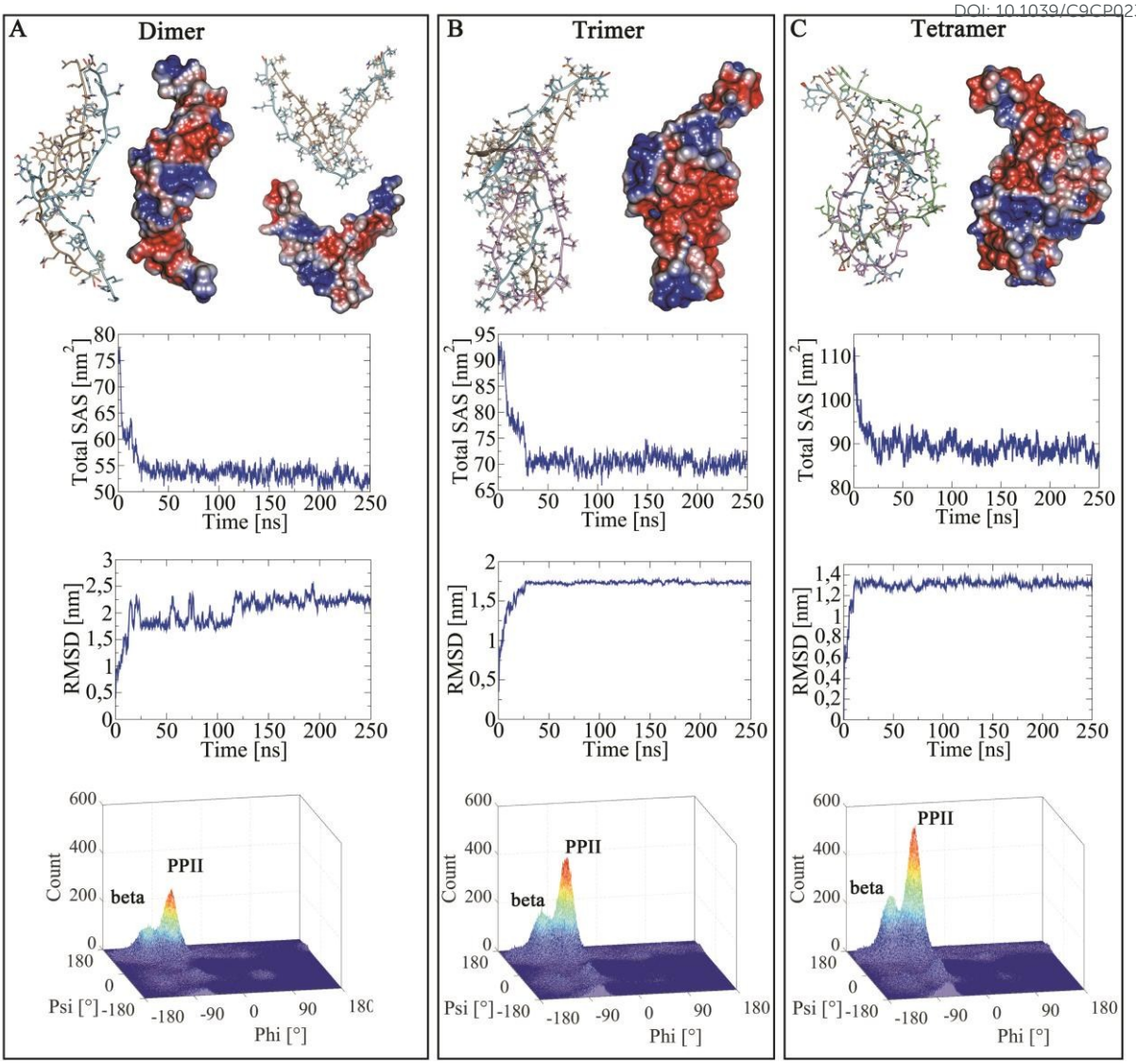

Figure 3. Molecular Dynamics Simulations and Analysis of the Secondary Structure of (A) Dimer, Trimer (B) and Tetramer (C), respectively. Top: Two Depictions of the most representative structures. The second corresponds to the molecular surface coloured by the electrostatic potential. Middle: Solvent accessible surface area and root-mean-square deviation through the MD simulation. Bottom: Ramachandran histogram of the trajectory of the corresponding simulations. (A) Dimer: The steep negative slope of the curve during the first nanoseconds represents the initial approach of the monomers and formation of a primitive dimer. It later evolves into a more compact structure but remains elongated for the rest of the simulation. The radius of gyration plot (Fig. S8) and additional orientations (Fig. S7) are in SI. (B) Trimer: Two steep negative slopes are observed at ~10 ns and ~30 ns. The first represents the aggregation of the trimer, while the second (smaller) represents an additional folding step. The radius of gyration plot (Fig. S10) and additional orientations (Fig. S11) are in SI. (C) Tetramer: The initial decrease corresponds to the formation of the tetramer, which is stable afterwards. The radius of gyration plot (Fig. S13) and additional orientations (Fig. S14) are in SI.

The exposed surface decreased as a consequence of the aggregation process during the first nanoseconds, then it reached a 20 ns plateau representing the intermediate conformation with the monomer exhibiting a free end, and finally, there was a decrease in the SAS area produced by this end folding towards the rest of the structure. After that, the trimer remained overall stable and elongated (Fig. S11). The clustering process generated 60 groups; the largest contained 90% of the total structures with an average RMSD with the main structure of 0.22 nm. The representative structure of the most important cluster, which corresponds to 203 ns, is shown in Figure 3B, and the H-bonds that stabilise such conformation are listed in Table S6, the evolution of the number of H-bonds is depicted in Fig S12. The overall shape is conserved after ~40ns.

In the same way, the formation of a tetramer from the interaction between an elongated monomer and a trimer was analysed. The MD simulation showed a quick aggregation of the trimer and the

monomer, and then the structure of the new tetramer remained stable, as represented by the SAS plot, the RMSD (Figure 3C) and the radius of gyration (Figure S13). The production run was clustered into 42 groups, the largest containing 58% of all the structures and an RMSD between the representative structure (152ns) and the remaining members of the cluster of 0.22 nm. This conformation of the tetramer (Figure 3C) was stabilised by several H-bonds (Figure S15 and Table S7) and remained unchanged for the rest of the simulation.

Regarding the secondary structure for all the oligomers, the Ramachandran histograms showed that the residues scattered mainly in the regions corresponding to β structures and PPII (Figures 2H, 3 A-C and S16).

Only a couple of amino acids display at some point dihedral angles which describe alpha-helices, which is statistically correct since the probability of this combination happening is very low because of the high proline content of the peptide. It was also observed that the higher the oligomer, the higher is the role of glutamine in the formation of stabilised H-bonds (Tables S4-7). Experimentally, the 33-mer peptide, on increasing concentration, exists as a mixture of PPII structure and β-structures.[6, 7] Here, we showed that during the MD simulations, the content of β structures increased, while the content of PPII decreased (from the starting monomer structure of 100% PPII) in all oligomers except in the tetramer in which they remain constant (Fig. S16). This difference can be explained by the already equilibrated content of both structures in the starting configuration of the tetramer.

Dityrosine formation and stabilisation of 33-mer peptide oligomers at low concentration

The 33-mer gliadin peptide presents in its sequence three tyrosine (Y) residues, LQLQPFPQPQLP^{69}YPQPQLP^{76}YPQPQLP^{83}YPQPQPF. In general, the tyrosine amino acid leads to the formation of radicals under oxidative conditions. [44] Under this circumstance, dityrosine bonds would be formed only when two tyrosine moieties are at a distance less than 5 Å. Therefore formation of dityrosine cross-links would probe the existence of 33-mer small oligomers at a relevant physiological concentration. [45-46] The new covalent C-C bond in the ortho-ortho position of both phenolic groups of the tyrosine group is a chemical tool employed to stabilise covalently low molecular oligomers and protein intermediates. Furthermore, the dityrosine formation process is associated with some physiological processes such as in the formation of ligaments in insects but also with pathological processes in neurodegenerative diseases, atherosclerosis and ageing. [47-50] Interestingly, the dityrosine bond was found to be of key importance in the formation of alpha-synuclein oligomers. [51,-52] In this regard, it is possible to monitor this transformation because the dityrosine bond presents a characteristic fluorescent signal at 407 nm when it is excited at 320 nm. Thus, the new bond can be monitored in real-time by using fluorescence spectroscopy. [53-55]

Nevertheless, the formation of dityrosine bonds cannot be reproduced through classic MD simulations; it is possible to identify whether there are tyrosine groups that remain nearby (< 5 Å) during the MD simulations (Fig. 4A-C, S17). After close visual inspection of the contacts between tyrosine moieties of the simulated structures, we observed that in the monomer, all lateral tyrosine chains remained separated. On the contrary, the dimer, trimer and tetramer displayed three tyrosines nearby, which could potentially form a dityrosine bond, these are Tyr69 and Tyr76 from chain A and Tyr69 from chain B (Fig. 4A-B).

In addition to these tyrosines, the representative structure of the decamer presents other position, more peripheral, that includes Tyr69 of chain C and Tyr83 of chain D (Figure 4C).

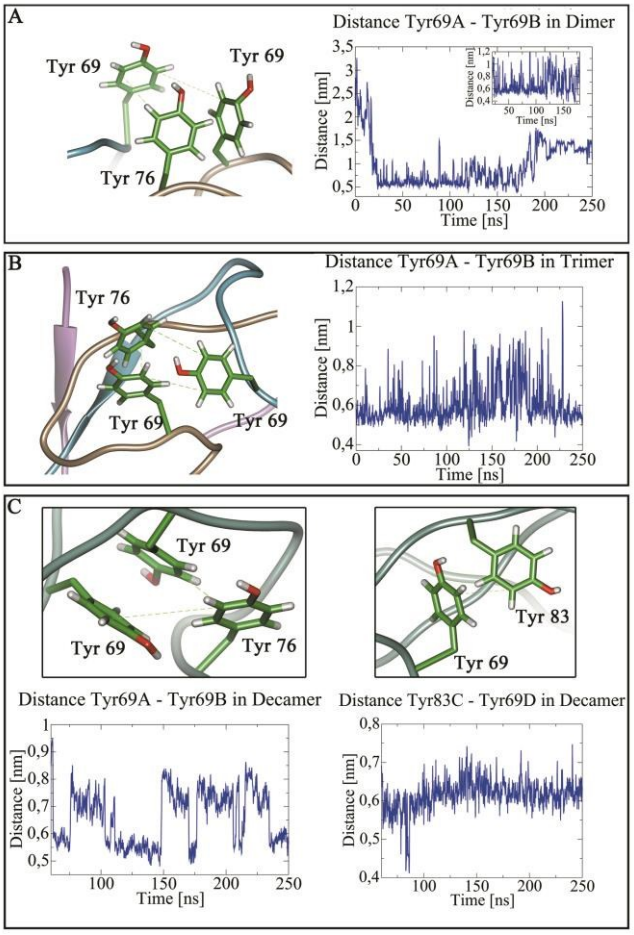

Figure 4. During the process of oligomerisation *in silico* two Tyr69 from different chains, together with a Tyr76 from one of those chains moved closer, reaching distances between their CZ atoms of ~ 0.5 nm, which is consistent with the plausible stabilisation of the oligomers through dityrosine bonds. (A) The depiction of the three tyrosines in the representative conformation of the dimer and plot of the distance between CZ atoms of Tyr69 from chain A and Tyr69 from chain B. (B) Representation of the same tyrosine in the representative structure of the trimer. (C) Both probable sites for dityrosine bond formation for the decamer are depicted together with the evolution of the distances between their CZ atoms.

The fact that the same assembly of tyrosines is observed in the dimer, trimer, tetramer and decamer, which were obtained from a different path, is suggestive of a conserved feature independent from the formation pathway. Taking into account these findings, we investigated the tyrosine cross-link of 33-mer at a concentration where oligomers were not observable by DLS. [6] The reaction was catalysed by the enzyme horseradish peroxidase at 37°C. The first objective was to immobilise and therefore identify the predicted low molecular weight 33-mer oligomers and second to elucidate if there is, experimentally, a preference in size. Previous to the oxidative reaction, the individual tyrosine spectra showed an emission maximum at 303 nm, as presented in Figure 5A. After the reaction; there was a decrease in the intensity at the 303 nm maximum, while a new band at 407 nm corresponding dityrosine was observed. Furthermore, the kinetics of the reaction was followed by exciting at 320 nm, which is specific for dityrosine moiety. The maximum production of this bond occurred during the first hour (Figure 5B), which was also corroborated by the characteristic emission spectra of the new dityrosine bond (Figure 5B inset). The size of the covalently linked 33-mer oligomers at 10, 20, 30 minutes and 1 hour was obtained by SDS gel electrophoresis (Figure 5C, see Materials and Methods). It was detected that at 10 and 20 minutes (lane 3 and 4, respectively), the main species in solution were monomer, dimers and trimers. However, after 30 minutes the presence of different oligomers from monomer to nonamers were detected; unfortunately, the corresponding band of the decamers (39110 Da) could not be detected because of the presence of the peroxidase which has the same MW (lane 5 and 6, respectively). These findings support our simulations and are indicative of a stepwise mechanism where different size oligomers co-exist in equilibrium with the monomer previous the nucleation event. To obtain information about the secondary structure of the 33-mer oligomers before (t0) and after the cross-linking reaction (t2h), we performed temperature-dependent circular dichroism experiments under both experimental conditions (Figure 6). Also, we corroborated that neither the presence of the enzyme nor the higher pH has a significant effect on the PPII secondary structure of 33-mer at the initial state (t0) (Fig. S18).

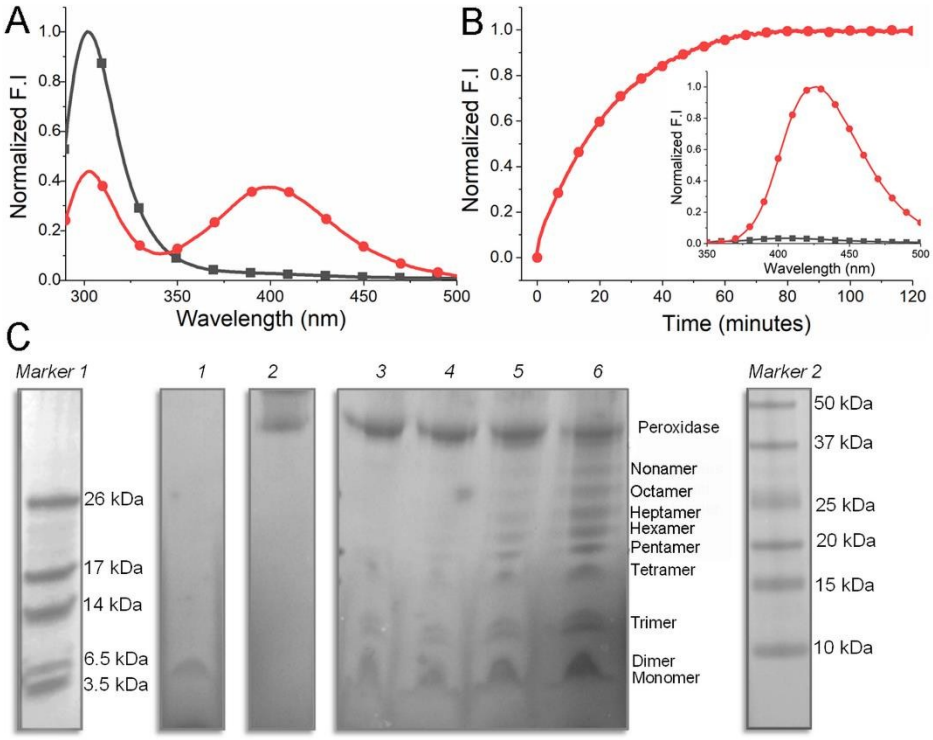

Figure 5. Analysis of the formation of 33-mer peptide oligomers stabilised by dityrosine bonds at 50 µM final concentration, pH 8.8 in borate buffer. (A) Emission spectra of tyrosine obtained by exciting the sample at 280 nm, before (■) and after (●) the reaction. (B) Time-dependent assay of dityrosine formation followed by emission fluorescence at 407 nm. In the insert, it is presented the dityrosine emission spectra before (■) and after the reaction occurs (●). In both experiments, the sample was excited at 320 nm. (C) Electrophoretic separation of 33-mer oligomers cross-linked by the formation of the dityrosine bond after different reaction times: 10 minutes (lane 3), 20 minutes (lane 4) and 30 minutes (lane 5) and 1 hour (lane 6). As controls, the 33-mer monomer without crosslinking (lane 1) and the horseradish peroxidase (lane 2) at the same concentration employed in the reaction and two different molecular weight markers were used. Analysis of the electrophoresis was performed and showed in the SI (Figure S19 and 20).

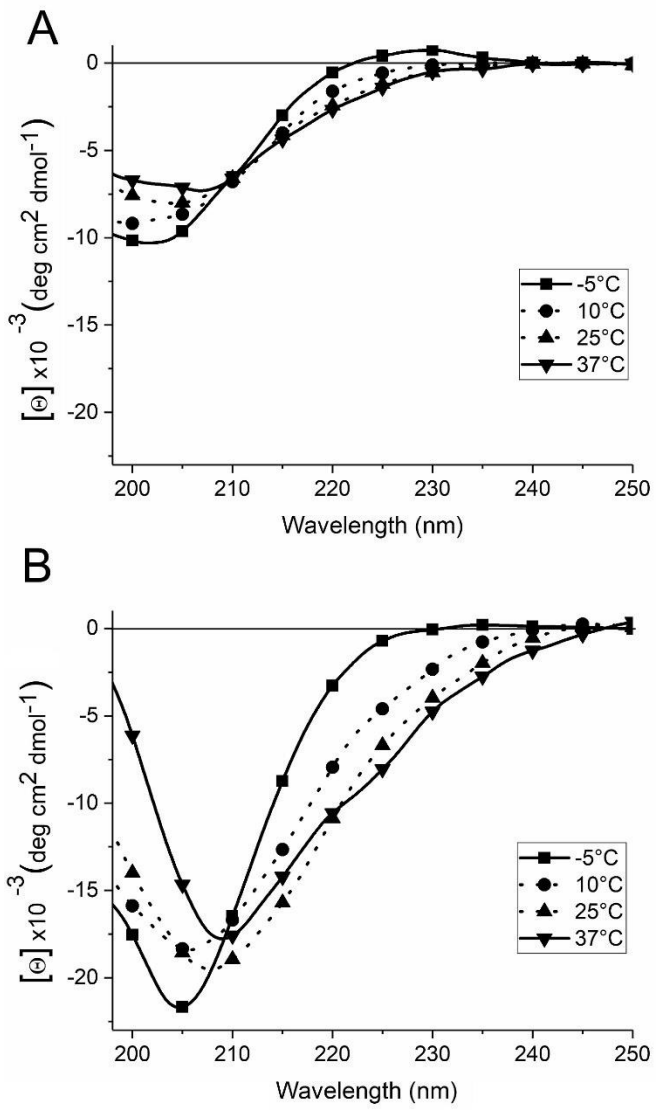

Figure 6. Circular Dichroism temperature-dependent experiments of 33-mer at 50 μM under crosslinking conditions. (A) At the initial time (t_0). (B) After 2h reaction (t_{2h}). For details, see materials and methods section.

Before the crosslinking reaction takes place, the 33-mer solution at 50 μM has a negative band at 202 nm and a small positive band at 228 nm at the lowest temperature of -5°C. This spectrum is characteristic of the PPII secondary structure (Fig. 6A). The PPII motif is characteristic of a negative band at around 200 nm and a small positive band at 220 nm, this last band is the signature of the PPII motif because it is absent in other secondary structures.[56,57] On the increasing temperature, the negative band became broad and shifted to 206 nm; meanwhile the 228 nm band became a negative shoulder. This behaviour was observed in and the 33-mer at concentrations below 197 μM and in other PPII model systems. [7, 57,58] Also, there was a hypochromic behaviour of the band at 202 nm from -10300 to -7300 deg cm^2 dmol^{-1}, on increasing temperature from -5 to 37°C (Fig. 6A). The presence of one isodichroic point at 210 nm implies that the 33-mer behaves as a two-state system in this temperature range. This experiment showed the loss of some PPII structure on increasing temperature, with an increase of the population of disordered states and/or the appearance of some small amount of β-structure, as observed before for native 33-mer and other model PPII peptides. [6, 7, 57, 58]

After the dityrosine crosslinking reaction, the 33-mer oligomers were covalently stabilised, and the system does not behave as a two-state system, as evidenced by the detected different isodichroic points (Fig. 6B). At the lowest temperature of -5°C, a negative band at 205 nm was observed with a value of molar ellipticity of 21600 deg cm^2 dmol^{-1}. Meanwhile, the value at 228 nm was nearly zero (-0.1600 deg cm^2 dmol^{-1}). Uversky has described that coil-like intrinsically disordered proteins (IDPs) that have substantial fractions of PPII helix displaying a molar ellipticity at around 200 nm of -19000± 2800 deg cm^2 dmol^{-1} and -1700 ±700 deg cm^2 dmol^{-1} at around 222 nm which are similar to the values observed for the 33-mer covalently bonded. [59] It seems that the covalent ensemble of 33-mer stabilises the formation of PPII helices. [57, 58] On increasing the temperature to 37°C, the negative minimum band shift to 209 nm with a decreased of molar ellipticity to -17500 deg cm^2 dmol^{-1}, observing a broad negative shoulder in the region above 220 nm. The shift of the minimum from 205 to 209 nm on increasing the temperature and the negative shoulder at 220 nm are indicative of a PPII structure in equilibrium to β structure. The BESTSEL algorithm was employed to compare the percentage of β-structure of the 33-mer covalent oligomers at-5°C and 37°C (Fig. 6B. complete line). [60] By doing this, it was shown that the β strand component increase when increasing the temperature from -5°C to 37°C. The increment of the β anti-parallel structure was from 47.5% to 61.5% and for the β parallel from 0 % to 7.5%. This algorithm is not suitable to quantify PPII content. [60]

Discussion

It is well-established that the primary structure of the proteolytical resistant 33-mer gliadin peptide may be relevant in the development of celiac disease and probably other gluten-related diseases. In this regard, the role of 33-mer oligomerisation as a trigger of diseases in humans remains elusive. Nevertheless, it has been shown that the large 33-mer superstructures activate the innate immune response in human macrophages by a TLR 4 mechanism.[9] Thus, the early steps of oligomerisation may be a novel therapeutic target to inhibit large oligomers formation thus avoiding the activation of the primary innate immune response.

Herein, we investigated the 33-mer oligomerisation using a combination of computational and experimental methods. Due to the highly repetitive sequence of 33-mer, NMR experiments, under physiologically relevant conditions, are challenging. Previously in deuterated dimethyl sulfoxide (DMSO-d^6), it had been shown that the 33-mer monomer has a PPII motif which was confirmed by CD spectroscopy. [4, 20] Later on, we showed that 33-mer secondary structure depends on concentration,

View Article Online
DOI: 10.1039/C9CP02338K

mainly due to the formation of different types of oligomers whose dimensions are from the nano- to the micrometer range. [6, 7, 9] Experimentally, the self-assembly process of 33-mer peptides is highly dependent on its concentration as determined by circular dichroism and ATR-FTIR spectroscopy. [6, 7] At low concentrations (between 6 and 50 μM), 33-mer exists in a conformational equilibrium between random and PPII secondary structure. Above 200 μM, the equilibrium shifts from PPII to parallel β-sheet structure.[6, 7] Both techniques evaluate the secondary structure of the sample as a whole and do not provide molecular information. The PPII secondary structure is characterised by the dihedral angles ϕ=- 75 and ψ= 145 in the Ramachandran plot. [20, 57] This motif has been related to intermediate states of protein folding and superstructure formation because the PPII conformation is always in equilibrium with others structures like β-turns, β-strands and unordered conformations; due to the proximity of the respective dihedral angle values. [61, 62] In the absence of further structural information about 33-mer oligomers, the initial configuration of 33-mer and its oligomers were computationally modelled. We began the *in silico* evaluation of the oligomerisation process with the analysis of ten monomers embedded in water. The starting structures were in extended PPII conformation since this was suggested by previous *in vitro* experiments. [4, 20] The atomistic MD simulation of the ten monomers showed that one monomer remained half of the simulation isolated and elongated, and it was possible to detect co-existence with a dimer and a heptamer to finally evolve into a decamer with increased β-structure content. The MD simulation of the monomer showed that during the first 25 ns it evolved as a stable elongated structure and after that, it began a folding process which resulted in a more compact structure with high β structure content. These outcomes suggested that during the early events of oligomerisation, a mixture of monomers in folded and extended configurations is statistically possible. Moreover, we showed that the partial charge distribution of the 33-mer monomer is not affected for the pH, as expected due to its non-ionic polar character; which correlates well with previous experimental results. In order to assess the plausibility of formation of 33-mer oligomers by a stepwise mechanism, different MD simulations with atomistic detail, between monomers and nearby lower-order oligomers were evaluated. Theoretically, it is possible the oligomerisation into dimers, trimers, tetramers and oligomers of a superior order, like decamers. All the oligomers displayed similar characteristics consistent with the experimental information obtained *in vitro*: i.e. secondary structures with a high content of PPII secondary structure in equilibrium with β structures and amphipathic characteristics. Furthermore, we detected an increase of H-bond formation among glutamines on increasing complexity, [63] justifying the observed stabilisation of the high order oligomers in water experimentally (Table S2-5). [6, 7, 9]

The aggregation into oligomers of a superior order indicated that different structures could survive in dynamical equilibrium, including those with larger architectures, as detected experimentally for the 33-mer by the mentioned microscopic techniques. This behaviour was described for other amylogenic oligomers, too. [63-66]

It is important to highlight that oligomerisation occurred for all the systems that were assessed. These results suggest that 33-mer gliadin peptide should exist as an oligomer in solution. Importantly, the dityrosine bonds are only possible when tyrosine moieties are in proximity less than 5Å. Formation of covalently bond 33-mer dityrosine oligomers was confirmed by the formation of a new emission band at 407 nm specific for dityrosine bond and the decrease of the maximum emission signal of tyrosine. Also, the kinetics of the dityrosine formation was followed by the emission of dityrosine at 407 nm. The cross-linked reaction reached the plateau after 1 hour. Furthermore, the MW of the 33-mer oligomers were determined by the electrophoretic separation under denatured conditions. The detection of monomers and oligomers of increasing MW from dimers to nonamers confirms the stepwise oligomerisation mechanism. As mentioned, the decamer could not be detected because of its similar MW with the peroxidase. We hypothesised based on our simulations that the dityrosine oligomers are formed through Tyr69 and Tyr76 as well as Tyr69 and Tyr83 of different monomeric chains.

The secondary structure evaluation by CD shows that before dityrosine crosslinking the 33-mer at the concentration of 50 μM behaves as a two-state system with a significant PPII structure in equilibrium with other secondary structures like random or β structures. This behaviour was described before for the 33-mer at low concentration. [6, 7] After the dityrosine crosslinking reaction, the 33-mer oligomers formed at 50 μM are covalently bonded, and the different size 33-mer oligomers remain stable in the buffer solution. Under this circumstance, the system increases its complexity, as shown for the different isodichroic points when the temperature increase. The PPII was detected as the main secondary structure at the lowest temperature tested, which then decreased its content in favour to β structures on increasing the temperature to 37°C. Interestingly, after cross-linking the covalent 33-mer ensemble showed a negative band at 205 nm, which is more than twofold relative to non-crosslinked system. We hypothesised that the formation of the Y-Y fixes the 33-mer in extended structures, thus considering the high content of prolines and glutamines of the system, the PPII helix is favoured. It is also accepted, that the PPII helices are favoured by intramolecular hydrogen bond from the glutamine side chain to the backbone carbonyl oxygen of the next residue of the sequence. [67] Taking into account that in the 33-mer sequence, the three tyrosine groups are located in the repetitive PYPQ sequence, it is highly probable that the new Y-Y favoured the mentioned intramolecular hydrogen bond. It seems that in the more flexible native 33-mer oligomers, intermolecular hydrogen bonds between the different interaction chains are favoured as obtained in the MD simulations.

The regular pattern of partial charge distribution along the peptide backbone obtained by MD shows the 33-mer amphiphilic nature of the monomer and oligomers even though the absence of ionic amino

acids. It is clear that the partial charge distribution on the monomer together with its flexible PPII structure is the driving force for the formation of the 33-mer oligomers. From the molecular point of view, the 33-mer peptide, LQLQPF(PQPQLPY)$_3$PQPQPF, contains 65% of proline (P) and glutamine (Q), suggesting that hydrophobicity could be the driving force for self-assembly. Nevertheless, we found hydrophobic patches in the decamer; the main driving force is the electrostatic distribution along with the polar non-ionic structure. Also, on increasing oligomer size, the Q residues stabilise the oligomer structure via complementary hydrogen bonding. Q can link beta-strands together into beta-sheets by a network of hydrogen bonds between the amides from the backbone and the polar side chains, as detected in the MD simulation. [68] The importance of Q lateral chain in the formation of protofilaments has been highlighted in different amylogenic diseases, including Huntington's disease.[69] Finally, P is known to form loops, which can trigger oligomerisation. By our simulations, we detect that the internal sequence ^{71}QPQL has a conserved β secondary structure. Thus, our simulations are meant to visualise the complementary partial charge distribution and rationalise the oligomerisation of the 33-mer peptide. Interestingly, dimerization as well as the formation of other oligomers, led to an increase of the polarisation of charge distribution along the new oligomer, facilitating further aggregation. The cross-linking experiment, together with our simulations showed that the stepwise mechanism is a feasible early oligomerisation pathway before the nucleation event (Scheme 2).

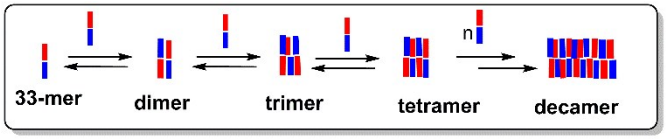

Scheme 2. Schematic representation of the stepwise oligomerisation pathway of 33-mer gliadin peptide promoted by complementary partial charge distribution.

The stepwise mechanism has been suggested for many homo-oligomeric proteins, which show the modulation of their biological activities by adjusting their oligomeric states. [64-66, 70.] Taking into account that electrostatics interactions influence or even dominate initial biochemical reactions.[71] The formation of different non-ionic polar 33-mer oligomers could potentially trigger different cellular responses. As observed microscopically, upon increasing peptide concentration, the interaction of different oligomers could lead to the nucleation step and formation of the 33-mer oligomers of a higher order. [6, 7, 9] We hypothesised that the propensity of 33-mer to oligomerize could explain its enzymatic proteolytical resistance. We are aware that further theoretical and experimental methodologies are needed to dissect the mechanism of 33-mer oligomerisation. Thus the relevance of our findings justifies further, more sophisticated approaches.[72, 73] Nevertheless, the trajectories showed an adequate sampling of the conformational space of each oligomer and provided the evidence that oligomerisation is statistically possible, as detected experimentally. Importantly, the atomistic simulations of 250 ns were sufficient to show the oligomerisation propensity with molecular detail. Furthermore, we validated the theoretical results experimentally using dityrosine crosslinking, isolating covalently bonded 33-mer small oligomers and detecting the presence of monomers, too.

Conclusions

In general, the combination of theoretical and experimental techniques in order to correlate molecular and supramolecular information is a clear win-win situation.[74] Here, taking advantage of this fact, we employed this interdisciplinary approach to elucidate the mechanisms of oligomerisation of the immunogenic 33-mer gliadin peptide. We demonstrated the existence of soluble small 33-mer oligomers experimentally, providing molecular details. Based on our findings, we hypothesised that the stepwise oligomerisation process occurs as the first event before 33-mer nucleation. The existence of different non-ionic polar 33-mer oligomers in the cellular environment might explain the different and sometimes unrelated pathological conditions that are triggered by gluten consumption.[1,2,5,8] Modulation of the early oligomerisation events may be crucial to delete the observed innate immune response triggered by the large 33-mer superstructures.[9] Therefore, inhibition of the early oligomerisation could be a novel therapeutic target. This report is a seminal contribution to disclose the role of 33-mer oligomers in gluten-related disorders at the molecular level. Finally, our report showed an unknown role of tyrosine to stabilise 33-mer small oligomers. Considering that oxidative conditions are a feasible environment in the inflammatory scenario. Thus, this plausible 33-mer metabolite needs to be further investigated by other biophysical tools and *in vivo*.

Conflicts of interest

There are no conflicts to declare.

Acknowledgements

This work was supported by the Alexander von Humboldt Foundation through a Georg Forster Fellowship to V.I.D and the German Academic Exchange Service through a fellowship to M.G.H. M.G.H. is also grateful for her CONICET fellowship. V.I.D. thanks Prof. Dr N. Sewald from Fakultät Chemie, Universität Bielefeld for his unconditional support

Notes and references

1. K. M. Lammers, M. G. Herrera and V. I. Dodero, *ChemistryOpen*, 2018, **7**, 217-232.
2. A. Sapone, J. C. Bai, C. Ciacci, J. Dolinsek, P. H. Green, M. Hadjivassiliou, K. Kaukinen, K. Rostami, D. S. Sanders, M. Schumann, R. Ullrich, D. Villalta, U. Volta, C. Catassi and A. Fasano, *BMC Medicine*, 2012, **10**, 13.

3. M. L. Moreno, A. Cebolla, A. Munoz-Suano, C. Carrillo-Carrion, I. Comino, A. Pizarro, F. Leon, A. Rodriguez-Herrera and C. Sousa, *Gut*, 2017, **66**, 250-257.
4. L. Shan, O. Molberg, I. Parrot, F. Hausch, F. Filiz, G. M. Gray, L. M. Sollid and C. Khosla, *Science*, 2002, **297**, 2275-2279.
5. B. Lebwohl, D. S. Sanders and P. H. R. Green, *Lancet*, 2018, **391**, 70-81.
6. M. G. Herrera, L. A. Benedini, C. Lonez, P. L. Schilardi, T. Hellweg, J. M. Ruysschaert and V. I. Dodero, *Soft Matter*, 2015, **11**, 8648-8660.
7. M. G. Herrera, F. Zamarreno, M. Costabel, H. Ritacco, A. Hutten, N. Sewald and V. I. Dodero, *Biopolymers*, 2014, **101**, 96-106.
8. S. W. Bruun, K. Josefsen, J. T. Tanassi, A. Marek, M. H. Pedersen, U. Sidenius, M. Haupt-Jorgensen, J. C. Antvorskov, J. Larsen, N. H. Heegaard and K. Buschard, *Journal of Diabetes Research*, 2016, **2016**, 2424306.
9. M. G. Herrera, M. Pizzuto, C. Lonez, K. Rott, A. Hutten, N. Sewald, J. M. Ruysschaert and V. I. Dodero, *Nanomedicine: Nanotechnology, Biology, and Medicine*, 2018, **14**, 1417-1427.
10. P. Tannous, H. Zhu, A. Nemchenko, J. M. Berry, J. L. Johnstone, J. M. Shelton, F. J. Miller, Jr., B. A. Rothermel and J. A. Hill, *Circulation*, 2008, **117**, 3070-3078.
11. C. M. Dobson, *Nature*, 2002, **418**, 729-730.
12. D. J. Selkoe, *Nature*, 2003, **426**, 900-904.
13. S. Campioni, B. Mannini, M. Zampagni, A. Pensalfini, C. Parrini, E. Evangelisti, A. Relini, M. Stefani, C. M. Dobson, C. Cecchi and F. Chiti, *Nature Chemical Biology*, 2010, **6**, 140-147.
14. M. Bucciantini, E. Giannoni, F. Chiti, F. Baroni, L. Formigli, J. Zurdo, N. Taddei, G. Ramponi, C. M. Dobson and M. Stefani, *Nature*, 2002, **416**, 507-511.
15. D. M. Walsh, I. Klyubin, J. V. Fadeeva, W. K. Cullen, R. Anwyl, M. S. Wolfe, M. J. Rowan and D. J. Selkoe, *Nature*, 2002, **416**, 535-539.
16. T. C. Michaels, A. J. Dear, J. B. Kirkegaard, K. L. Saar, D. A. Weitz and T. P. Knowles, *Physical Review Letters*, 2016, **116**, 258103.
17. L. Tran, N. Basdevant, C. Prévost and T. Ha-Duong, *Scientific Reports*, 2016, **6**, 21429.
18. M. Baram, Y. Atsmon-Raz, B. Ma, R. Nussinov and Y. Miller, *Physical Chemistry Chemical Physics*, 2016, **18**, 2330-2338.
19. L. Ning, J. Guo, Q. Bai, N. Jin, H. Liu and X. Yao, *PloS One*, 2014, **9**, e87266.
20. I. Parrot, P. C. Huang and C. Khosla, *The Journal of Biological chemistry*, 2002, **277**, 45572-45578.
21. B. Honig and A. Nicholls, *Science*, 1995, **268**, 1144-1149.
22. M. E. Davis and J. A. McCammon, *Chemical Reviews*, 1990, **90**, 509-521.
23. N. A. Baker, D. Sept, S. Joseph, M. J. Holst and J. A. McCammon, *Proceedings of the National Academy of Sciences of the United States of America*, 2001, **98**, 10037-10041.
24. T. J. Dolinsky, P. Czodrowski, H. Li, J. E. Nielsen, J. H. Jensen, G. Klebe and N. A. Baker, *Nucleic acids research*, 2007, **35**, W522-525.
25. T. J. Dolinsky, J. E. Nielsen, J. A. McCammon and N. A. Baker, *Nucleic acids research*, 2004, **32**, W665-667.
26. M. H. Olsson, C. R. Sondergaard, M. Rostkowski and J. H. Jensen, *Journal of chemical theory and computation*, 2011, **7**, 525-537.
27. C. R. Sondergaard, M. H. Olsson, M. Rostkowski and J. H. Jensen, *Journal of chemical theory and computation*, 2011, **7**, 2284-2295.
28. C. L. Tang, E. Alexov, A. M. Pyle and B. Honig, *Journal of molecular biology*, 2007, **366**, 1475-1496.
29. D. Sitkoff, K. A. Sharp and B. Honig, *The Journal of Physical Chemistry*, 1994, **98**, 1978-1988.
30. Z. Zhang, H. Chen, H. Bai and L. Lai, *Biophysical Journal*, 2007, **93**, 1484-1492.
31. A. Barducci, M. Bonomi, M. K. Prakash and M. Parrinello, *Proceedings of the National Academy of Sciences of the United States of America*, 2013, **110**, E4708-4713.
32. S. Páll, M. J. Abraham, C. Kutzner, B. Hess and E. Lindahl, Cham, 2015.
33. H. J. C. Berendsen, D. van der Spoel and R. van Drunen, *Computer Physics Communications*, 1995, **91**, 43-56.
34. C. Oostenbrink, A. Villa, A. E. Mark and W. F. van Gunsteren, *Journal of computational chemistry*, 2004, **25**, 1656-1676.
35. H. J. C. Berendsen, J. R. Grigera and T. P. Straatsma, *The Journal of Physical Chemistry*, 1987, **91**, 6269-6271.
36. W. G. Hoover, *Physical Review A*, 1985, **31**, 1695-1697.
37. S. Nosé, *Molecular Physics*, 1984, **52**, 255-268.
38. M. Parrinello and A. Rahman, *Journal of Applied Physics*, 1981, **52**, 7182-7190.
39. T. Darden, D. York and L. Pedersen, *The Journal of Chemical Physics*, 1993, **98**, 10089-10092.
40. B. Hess, H. Bekker, H. J. C. Berendsen and J. G. E. M. Fraaije, *Journal of computational chemistry*, 1998, **18**, 1463-1472.
41. J. E. J. Mills and P. M. Dean, *Journal of Computer-Aided Molecular Design*, 1996, **10**, 607-622.
42. D. Frishman and P. Argos, *Proteins*, 1995, **23**, 566-579.
43. C. Fernandez-Patron, in *The Protein Protocols Handbook*, ed. J. M. Walker, Humana Press, Totowa, NJ, 2002, DOI: 10.1385/1-59259-169-8:251, pp. 251-258.
44. M. T. Neves-Petersen, S. Klitgaard, T. Pascher, E. Skovsen, T. Polivka, A. Yartsev, V. Sundstrom and S. B. Petersen, *Biophysical Journal*, 2009, **97**, 211-226.
45. R. Aeschbach, R. Amado and H. Neukom, *Biochimica et Biophysica Acta*, 1976, **439**, 292-301.
46. M. Correia, M. T. Neves-Petersen, P. B. Jeppesen, S. Gregersen and S. B. Petersen, *PloS One*, 2012, **7**, e50733.
47. C. Giulivi and K. J. A. Davies, in *Methods in Enzymology*, Academic Press, 1994, vol. 233, pp. 363-371.
48. S. O. Andersen, *Biochimica et Biophysica Acta (BBA) - General Subjects*, 1964, **93**, 213-215.
49. S. Pennathur, V. Jackson-Lewis, S. Przedborski and J. W. Heinecke, *The Journal of Biological Chemistry*, 1999, **274**, 34621-34628.
50. C. Leeuwenburgh, J. E. Rasmussen, F. F. Hsu, D. M. Mueller, S. Pennathur and J. W. Heinecke, *The Journal of Biological Chemistry*, 1997, **272**, 3520-3526.
51. Y. Kato, W. Maruyama, M. Naoi, Y. Hashizume and T. Osawa, *FEBS letters*, 1998, **439**, 231-234.

View Article Online
DOI: 10.1039/C9CP02338K

52. Y. K. Al-Hilaly, T. L. Williams, M. Stewart-Parker, L. Ford, E. Skaria, M. Cole, W. G. Bucher, K. L. Morris, A. A. Sada, J. R. Thorpe and L. C. Serpell, *Acta Neuropathologica Comm.*, 2013, **1**, 83.
53. Y. K. Al-Hilaly, L. Biasetti, B. J. Blakeman, S. J. Pollack, S. Zibaee, A. Abdul-Sada, J. R. Thorpe, W. F. Xue and L. C. Serpell, *Scientific Reports*, 2016, **6**, 39171.
54. M. M. Wördehoff, H. ShaykHalishahi, L. Groß, L. Gremer, M. Stoldt, A. K. Buell, D. Willbold, W. Hoyer, *J Mol Biol.* 2017 **13**, 3018-3030.
55. D. A. Malencik and S. R. Anderson, *Amino acids*, 2003, **25**, 233-247.
56. V. I. Dodero, Z. B. Quirolo, M. A. Sequeira, *Frontiers in Bioscience*, 2011, **16**, 61-73.
57. R. W. Woody, Circular Dichroism of intrinsically disordered proteins, in Instrumental Analysis of Intrinsically Disordered Proteins: Assessing Structure and Conformation, John Wiley &Sons, Inc., 2010.
58. A. L. Rucker and T. P. Creamer, *Protein Sci.*, 2002, **11**, 980-985.
59. Uversky V. N., *Protein Sci.*, 2002, **11**, 739-75.
60. A. Micsonai, F. Wien, E. Bulyaki, J. Kun, E. Moussong, Y. H. Lee, Y. Goto, M. Refregiers and J. Kardos, *Nucleic Acids Research*, 2018, **46**, W315-W322.
61. B. J. Stapley and T. P. Creamer, *Protein Sci.,* 1999, **8**, 587-595.
62. L. D. Muiznieks and F. W. Keeley, *The Journal of Biological Chemistry*, 2010, **285**, 39779-39789.
63. M. Srinivasan and A. K. Dunker, *International Journal of Peptides*, 2012, **2012**, 634769.
64. N. H. Rhys, A. K. Soper and L. Dougan, *The Journal of Physical Chemistry. B*, 2012, **116**, 13308-13319.
65. X. Li, C. Dong, M. Hoffmann, C. R. Garen, L. M. Cortez, N. O. Petersen and M. T. Woodside, *Scientific Reports,* 2019*,* **9**, 1734.
66. S. Nag, B. Sarkar, A. Bandyopadhyay, B. Sahoo, V. K. A. Sreenivasan, M. Kombrabail, C. Muralidharan and S. Maiti, The *Journal of Biological Chemistry*, 2011, **286**, 13827-13833.
67. T. P. Creamer and M. N. Campbell, *Advances in Protein Chemistry*, 2002, **62**, 263-282.
68. Y. E. Kim, F. Hosp, F. Frottin, H. Ge, M. Mann, M. Hayer-Hartl, and F. U. Hartl, *Molecular Cell*, 2016, **63**, 951–964.
69. D. Punihaole, R.J. Workman, Z. Hong, J.D Madura and S.A Asher, *J Phys Chem B,* 2016, **120**, 3012-3026.
70. H. T Zoghbi and H. T. Orr, A*nnu. Rev. Neurosci.,* 2000, **23**, 217-247.
71. Y. Feng, W. Jiao, X.Fu, and Z. Chang, *Protein Sci*. 2006, **15,** 1441–1448.
72. Honig, H.; Nicholls, A. Science 1995, **268**, 1144-1149.
73. C. Frieden, *Protein Sci,* 2007, **16**, 2334-2344.
74. P. W. J. M. Frederix, I. Patmanidis, S. J. Marrink., *Chem. Soc. Rev*., **2018**, 47, 3470-3489

Table of content entry

View Article Online
DOI: 10.1039/C9CP02338K

The 33-mer gliadin peptide oligomerizes driving by its non-ionic polar character, flexible PPII secondary structure and stable glutamine H-bonds.

View Article Online
DOI: 10.1039/C9CP02338K

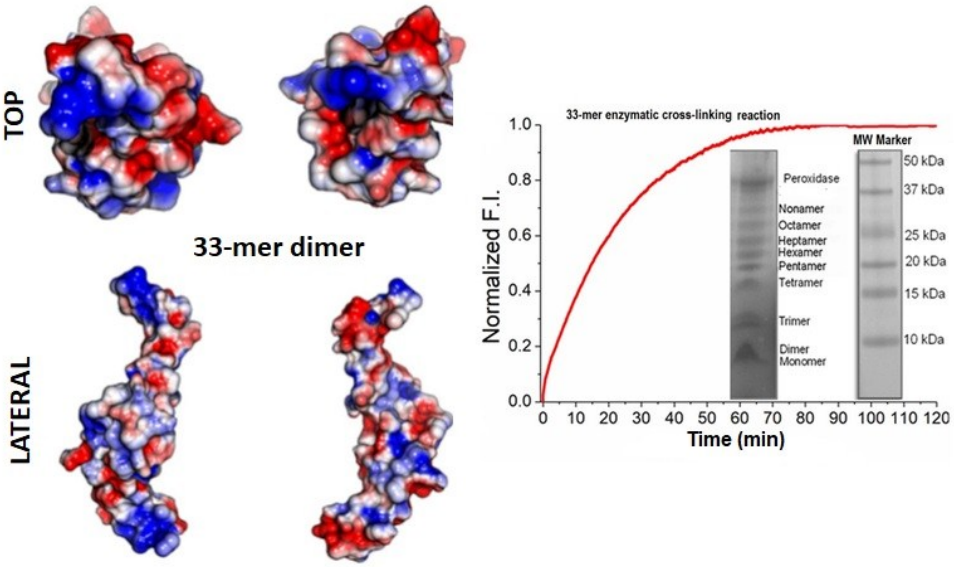

Table of Content Figure

67x39mm (300 x 300 DPI)